SUPPLEMENTARY INFORMATION

The Relative Impact of Ligand Flexibility and Redox Potential on the Activity of Cu Superoxide Dismutase Mimics

Sharon Signorella, Micaela Bruno, Gianfranco Frattini, Claudia Palopoli, Diego Moreno, Nora Pellegri, Verónica Daier and Sandra R. Signorella

Table of contents

Table S1. Crystal data and structure refinement for [Cu(salbn)] and $[Cu(py_2pn)(OAc)]ClO_4$

Empirical formula	$C_{18}H_{18}CuN_2O_2$	$C_{18}H_{21}ClCuN_4O_6$
Formula weight	357.89	488.38
Temperature	298(2) K	298(2) K
Wavelength	0.71073 Å	0.71073 Å
Crystal system, space group	Orthorhombic, P b c a	Monoclinic, P 21/n
Unit cell dimensions	a = 10.3829(10) Å α = 90º	a = 7.0578(8) Å α = 90º
	b = 14.7619(16) Å β = 90º	b = 24.333(3) Å β = 102.707º
	c = 20.471(2) Å γ = 90º	c = 12.4664(13) Å γ = 90º
Volume	3137.6(5) $Å^3$	2088.5(4) $Å^3$
Z, Calculated density	8, 1.515 g/cm^3	4, 1.553 g/cm^3
Absorption coefficient	1.403 mm^{-1}	1.216 mm^{-1}
F(000)	1480	1004
Crystal size	0.200 x 0.340 x 0.472 mm	0.040 x 0.104 x 0.128 mm
Theta range for data collection	2.597 to 26.355 deg	1.872 to 25.479 deg
Limiting indices	-12<=h<=12, -18<=k<=18, -24<=l<=25	-8<=h<=8, -29<=k<=29, -15<=l<=15
Reflections collected / unique	28695 / 3196 [R(int) = 0.043]	51971 / 3843 [R(int) = 0.1450]
Completeness to theta = 25.24	99.9 %	100.0 %
Refinement method	Full-matrix least-squares on F^2	Full-matrix least-squares on F^2
Data / restraints / parameters	3196 / 0 / 208	3843 / 12 / 282
Goodness-of-fit on F^2	1.024	1.196
Final R indices [I>2sigma(I)]	R1 = 0.0286, wR2 = 0.0669	R1 = 0.0952, wR2 = 0.2113
R indices (all data)	R1 = 0.0410, wR2 = 0.0723	R1 = 0.1227, wR2 = 0.2255
Largest diff. peak and hole	0.229 and -0.34 $e.Å^{-3}$	0.932 and -0.666 $e.Å^{-3}$

Table S2. Selected bond lengths (Å) and angles (°) for [Cu(salbn)]

Cu1-O1	1.8980(15)	O1-Cu1-O1'	87.77(7)	O1-Cu1-N1	93.47(7)
Cu1-N1	1.9405(16)	O1'-Cu1-N1	144.21(7)	O1-Cu1-N1’	153.25(7)
Cu1-O1'	1.9064(14)	O1'-Cu1-N1'	94.03(7)	N1-Cu1-N1’	100.33(7)
Cu1-N1'	1.9880(17)				

Standard deviations in parentheses. Symmetry transformations used to generate equivalent atoms: –x+1, -y+1, z.

Table S3. Selected bond lengths (Å) and angles (°) for the crystal and optimized structures of $[Cu(py_2bn)(X)]^{2+/+}$

Distances (Å)	$[Cu(py_2bn)(OAc)]ClO_4$ Crystal (experim)	$[Cu(py_2bn)(OAc)]^+$ in DMF (calc)	$[Cu(py_2bn)(HOAc)]^{2+}$ in water (calc)	$[Cu(py_2bn)(H_2O)]^{2+}$ in water (calc)
Cu-N(1)	2.016(6)	2.027	2.001	2.005
Cu-N(2)	2.006(6)	2.032	2.030	2.036
Cu-N(2')	2.030(6)	2.027	1.984	1.986
Cu-N(1')	2.237(6)	2.295	2.100	2.111
Cu-O(1)	1.934(5)	1.951	2.128	-
Cu-O(2)	2.754(5)	2.741	-	-
Cu-O(3)		-	-	2.085
Angles (°)				
N(1')-Cu-N(1)	103.0(2)	106.5	101.4	100.5
N(1')-Cu-N(2')	77.4(2)	77.7	81.4	81
N(1')-Cu-N(2)	102.7(2)	104.7	122.7	120.4
N(1')-Cu-O(1)	91.8(2)	91.3	115.5	-
N(1')-Cu-O(3)	-	-	-	114.4
N(2)-Cu-N(2')	90.7(3)	90.6	93.4	93
N(2')-Cu-O(1)	96.5(2)	95.2	93.5	-
N(2')-Cu-O(2)	91.4(2)	89.1	-	-
N(2')-Cu-O(3)		-	-	90.6
N(2)-Cu-N(1)	80.9(2)	80.6	81.5	81.4
N(2)-Cu-O(1)	165.0(2)	-	121.8	-
N(2)-Cu-O(2)	114.1(2)	111.3	-	-
N(2)-Cu-O(3)	-	-	-	125
N(1)-Cu-O(1)	92.0(2)	92.8	89.1	-
N(1)-Cu-O(2)	93.1(2)	92.1	-	-
N(1)-Cu-O(3)	-	-	-	93.8
O(1)-Cu-O(2)	52.74(17)	53.9		

Standard deviations in parentheses.

Table S4. Redox potentials of Cu(II) complexes under study

Complex	Solvent	$E(II/I)_{1/2}$ vs Fc^+/Fc^0 (mV)	E(II/I) vs *SCE* (mV)	Solvent	$E(II/I)_{pc}$ vs *SCE* (mV)
[Cu(salbn)]	MeCN	-1,368	-980	H_2O, pH 7.8*	-361 (E_{pc})
	DMF	-1,375	-901		
	MeOH	-1,027	-618		
$[Cu(py_2bn)(OAc)]ClO_4$	MeCN	-295	93	H_2O, pH 7.8*	-229 (E_{pc})
	MeOH	-293	116		

*Reduction potential of the Zobell's solution = 185 mV *vs SCE*

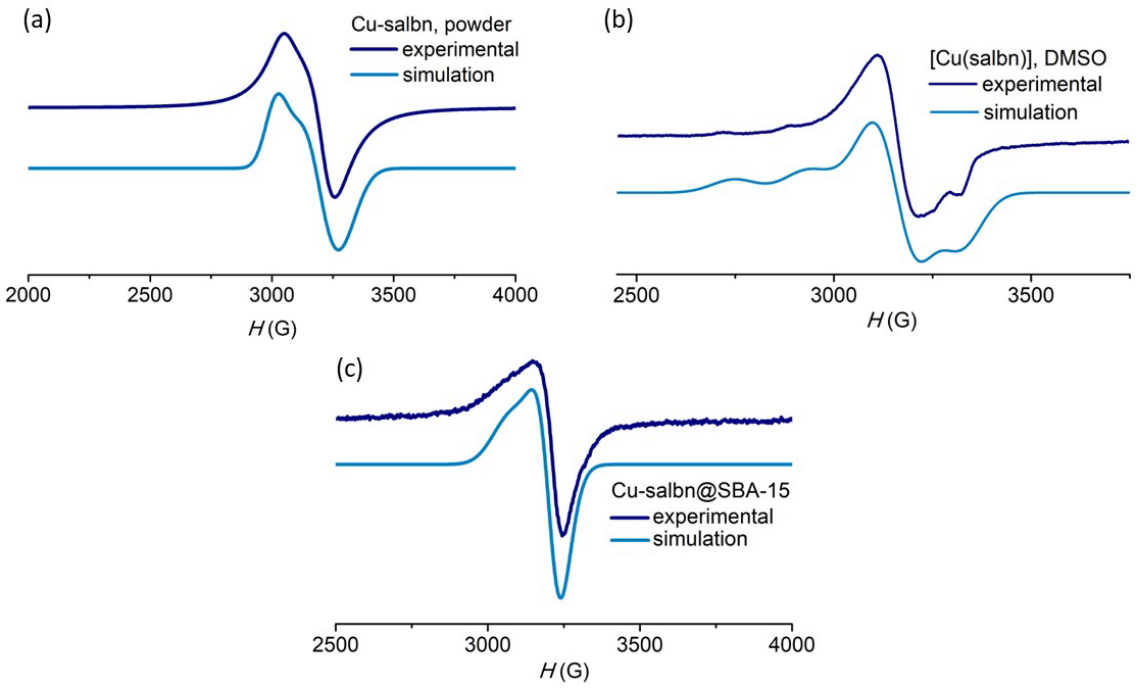

Figure S1. Experimental and simulated X-band EPR spectra of (a) powdered and (b) frozen DMSO solution of [Cu(salbn)], and (c) Cu-salbn@SBA-15. *T* = 120 K

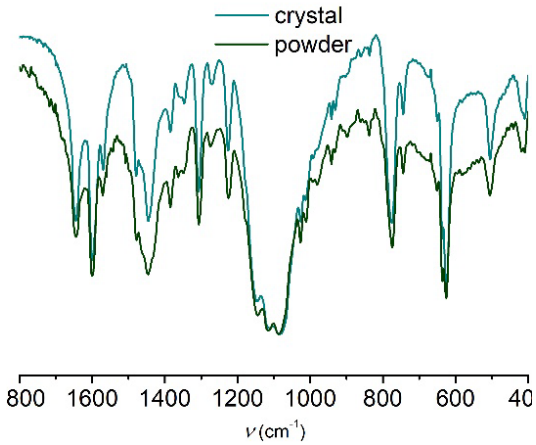

Figure S2. FT-IR spectra of crystals and powdered samples of $[Cu(py_2bn)(OAc)]ClO_4$

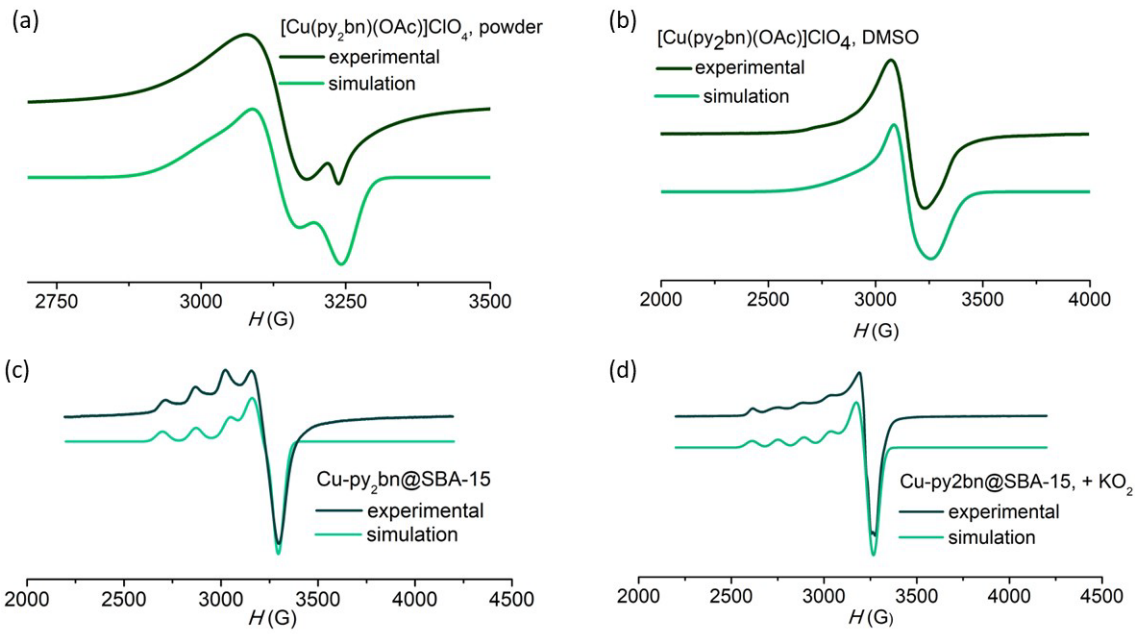

Figure S3. Experimental and simulated X-band EPR spectra of (a) powdered, (b) frozen DMSO solution of [Cu(py$_2$bn)(OAc]ClO$_4$, and Cu-py$_2$bn@SBA-15 before (c) and after (d) reaction with excess KO$_2$. *T* =120 K

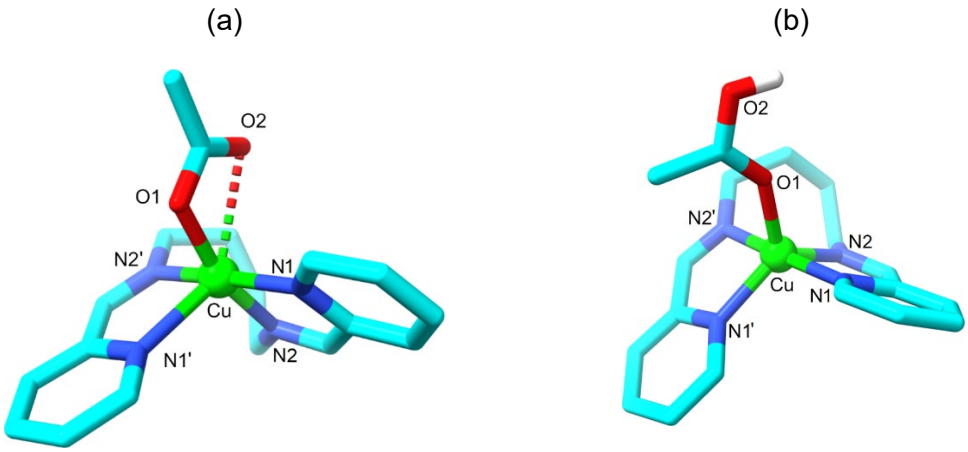

Figure S4. Optimized structure of a) [Cu(py$_2$bn)(OAc)]$^+$ in DMF and b) [Cu(py$_2$bn)(HOAc)]$^{2+}$ in water showing the change in coordination mode of the acetate ligand due to its protonation. Carbon atoms are shown in cyan, nitrogen atoms are shown in blue, copper atoms are shown in green and oxygen atoms are shown in red. For clarity, H atoms have been omitted

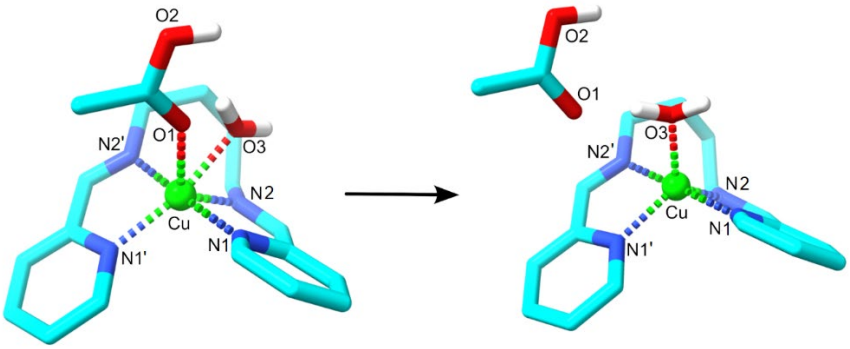

Figure S5. Visualization of the exchange of the acetate ligand for a H_2O molecule in water as a solvent. On the left, the initial state with water equidistant from the copper ion with respect to the acetate ligand. On the right, the optimized structure in which the substitution of ligand is observed. Carbon atoms are shown in cyan, nitrogen atoms are shown in blue, copper atoms are shown in green, oxygen atoms are shown in red and hydrogen atom in white. For clarity, H atoms have been omitted

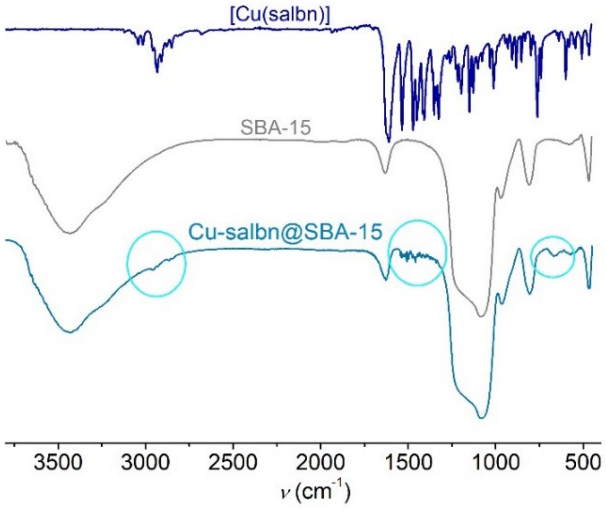

Figure S6. IR spectra of Cu-salbn, SBA-15 and hybrid material. Circles: bands from the catalyst

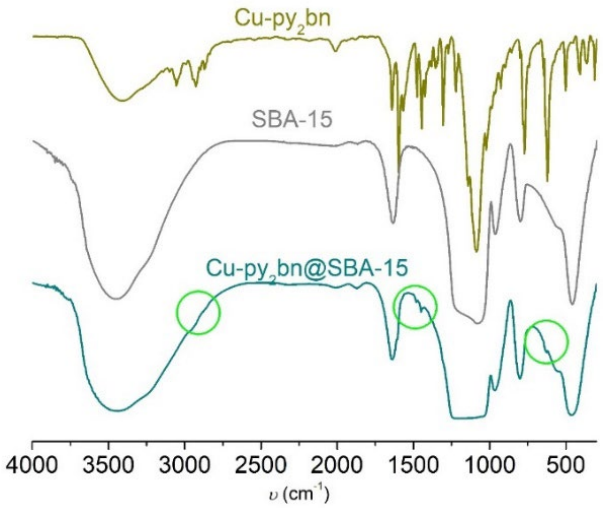

Figure S7. IR spectra of Cu-py$_2$bn, SBA-15 and hybrid material. Circles: bands from the catalyst

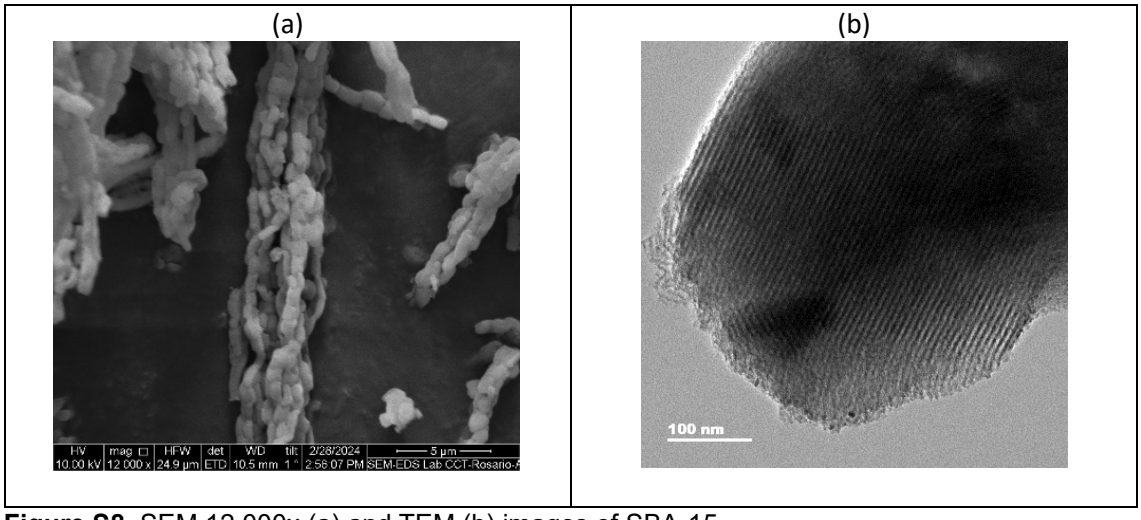

Figure S8. SEM 12,000x (a) and TEM (b) images of SBA-15

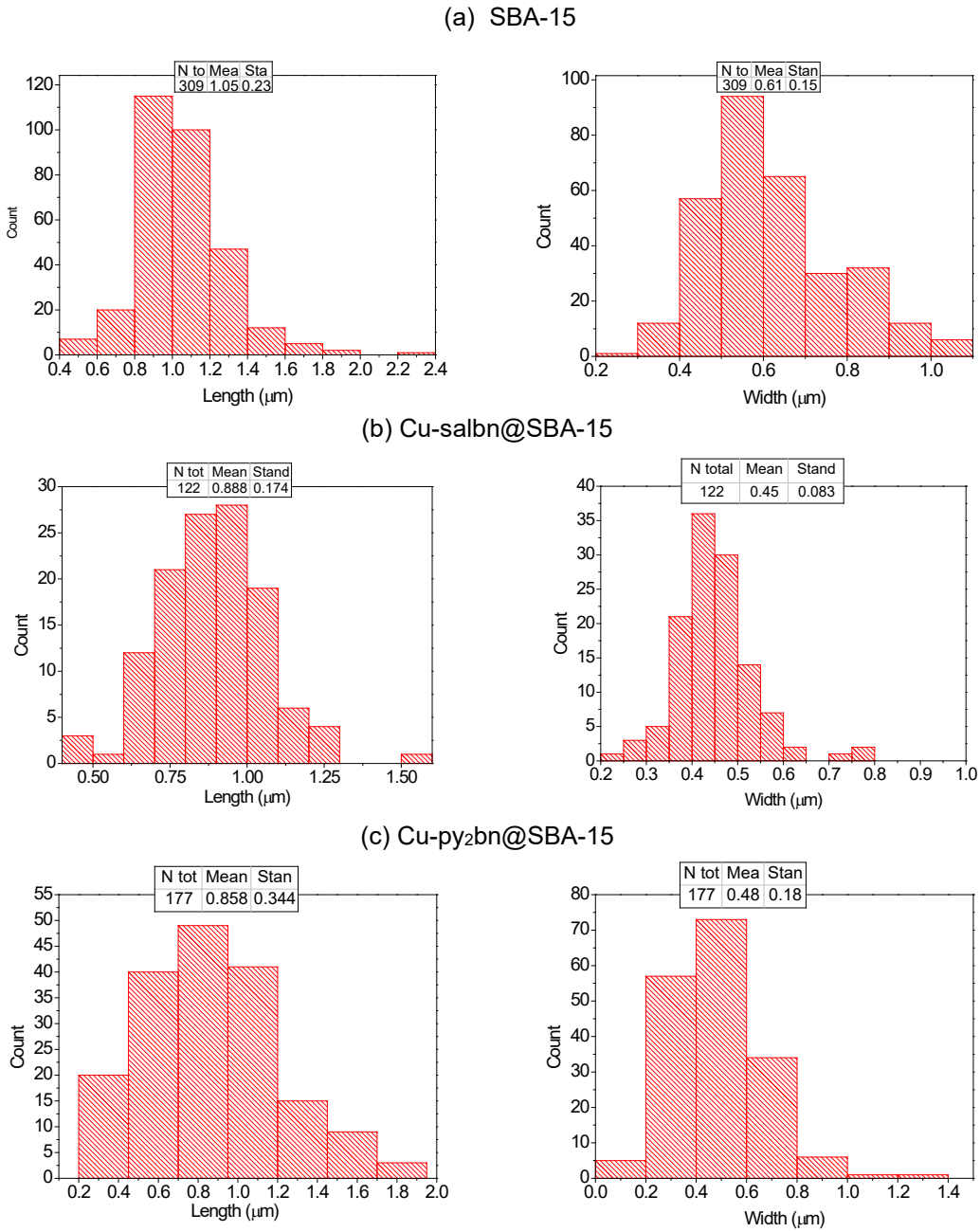

Figure S9. Histograms of length and width distribution for selected particles of mesoporous materials

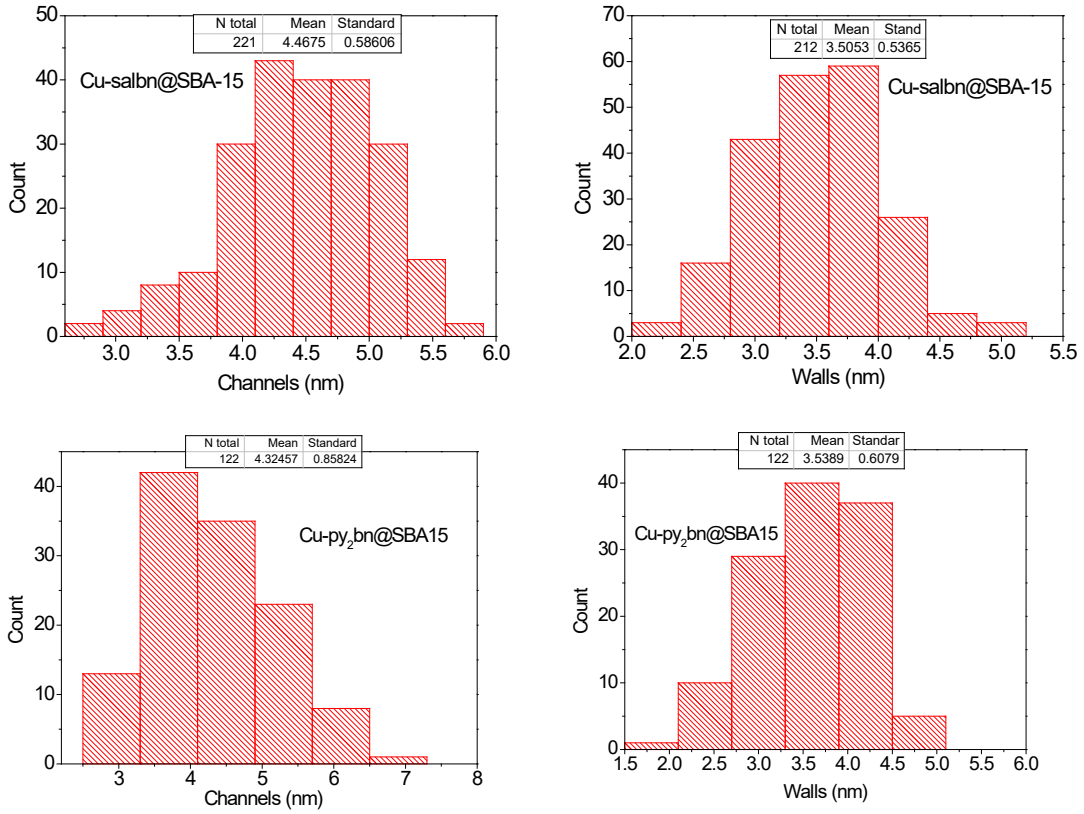

Figure S10. Histograms of the channel diameter and wall thickness of Cu-salbn@SBA-15 and Cu-py$_2$bn@SBA-15

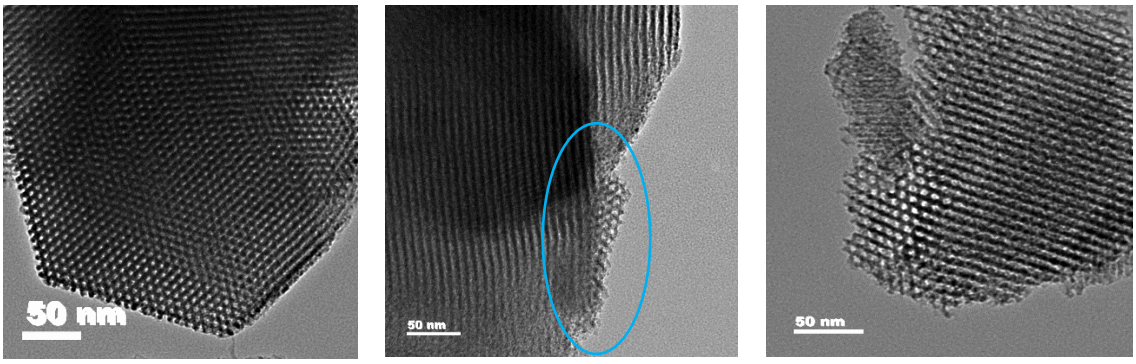

Figure S11. TEM images of hybrid materials showing the hexagonal arrangement of channels in SBA-15, Cu-salbn@SBA-15 and Cu-py$_2$bn@SBA-15

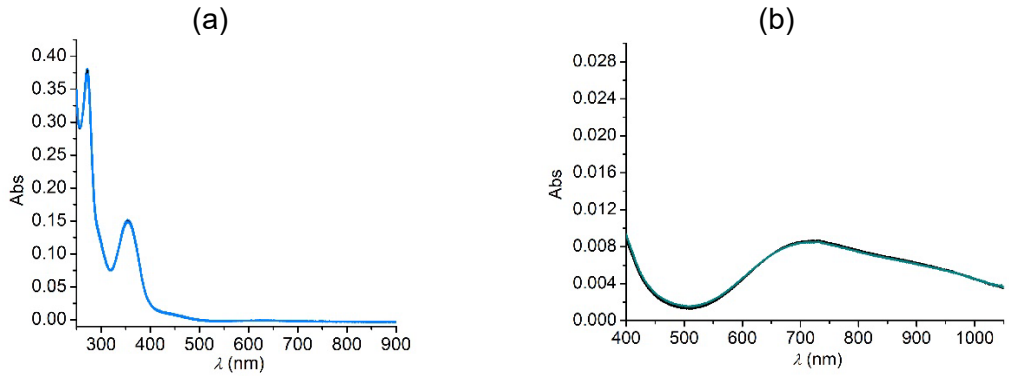

Figure S12. Successive UV-vis spectra of a) 0.014 mM [Cu(salbn)] and b) 0.078 mM [Cu(py$_2$bn)], in 0.2 M $HPO_4^{2-}/H_2PO_4^-$ buffer, pH = 7.8, during 2 h.

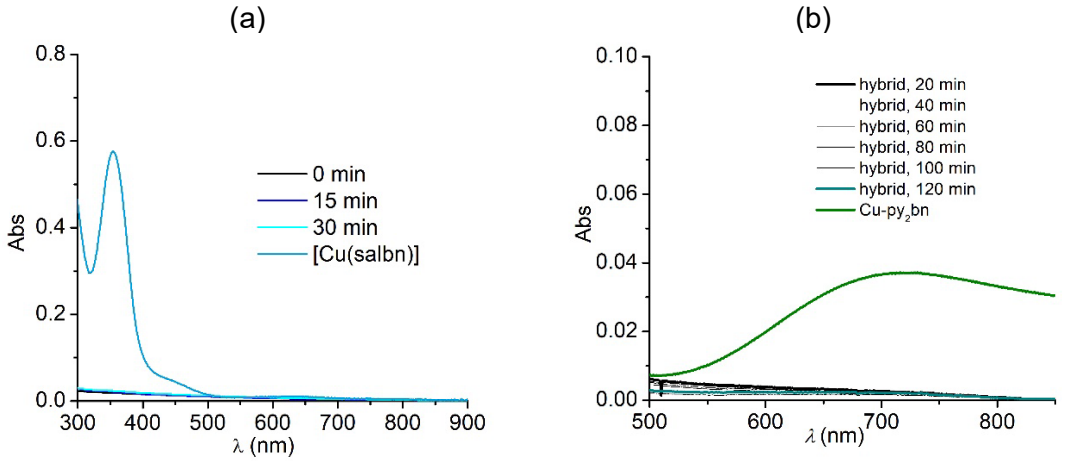

Figure S13. Electronic spectra of supernatant of hybrid suspensions after several incubation times in phosphate buffer of pH 7.8. (a) 1.0 mg/mL Cu-salbn@SBA-15, 0.05 mM [Cu(salbn)]; (b) 1.2 mg/mL Cu-py$_2$bn@SBA-15, 0.33 mM $[Cu(py_2bn)]^{2+}$.

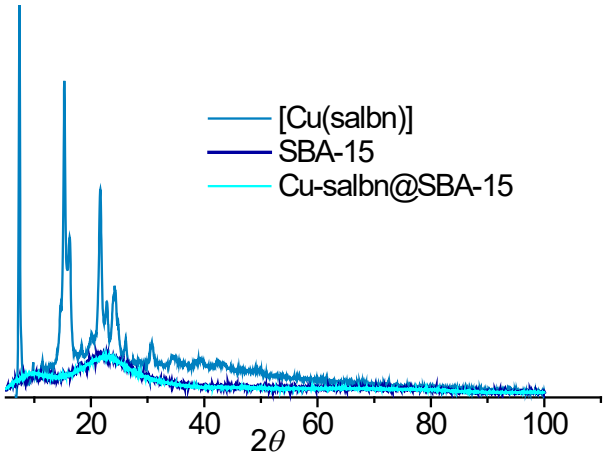

Figure S14. High angle X-ray diffractograms of powdered and encapsulated [Cu(salbn)]

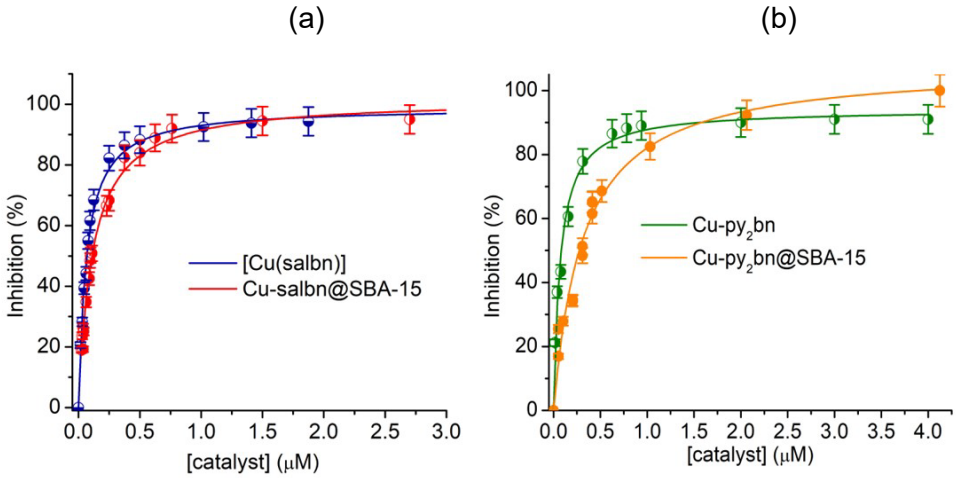

Figure S15. SOD activity of free and immobilized catalysts

Synthesis of [Cu(salpn)]. To a solution of 216 mg of Cu(OAc)·H_2O (1.08 mmol) in methanol (24 mL), were added 312 mg of H_2salpn (1.1 mmol), and the mixture was reacted with stirring at reflux, for 2 h. After cooling at room temperature, the green crystalline solid was filtered, washed with cold methanol and hexane, and dried under vacuum. Yield: 274 mg (0.80 mmol, 74%). Anal. calcd. for $C_{17}H_{16}CuN_2O_2$: C 59.4, Cu 18.5, H 4.7, N 8.1%; Found: C 59.1, Cu 18.7 H 4.5, N 8.2%. Significant IR bands (KBr, ν, cm^{-1}): 3022, 2907, 1605, 1537, 1470, 1327, 1125, 746. ESI-MS: m/z = 343.5.

Chart S1. Structures of ligands listed in Table 2

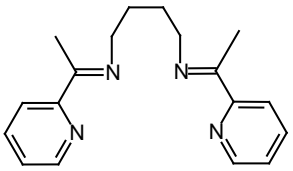

aptn

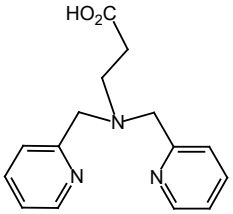

HPBMPA

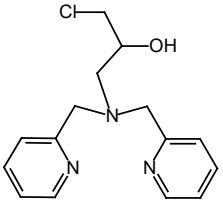

HPClNOL

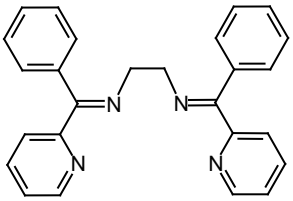

L^1

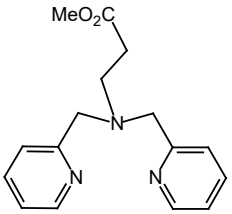

MPBMPA

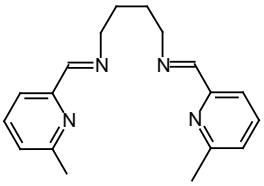

Pu-6-MePy

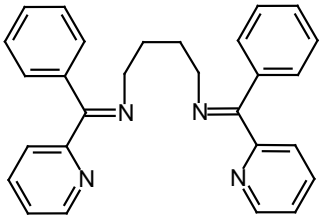

PuPhePy

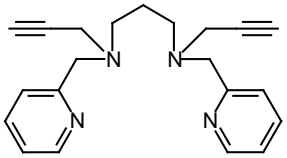

pypapn

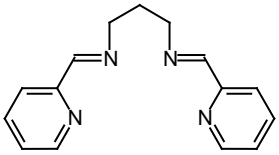

py_2pn

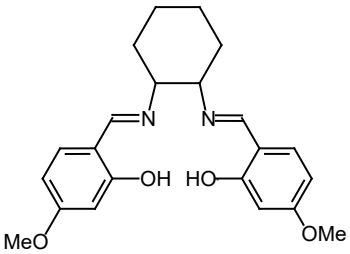

4-OMe-salen

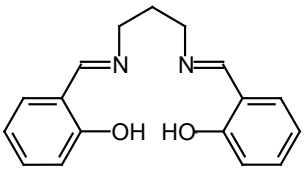

salpn